One-Step Homogeneous Magnetic Nanoparticle Immunoassay for Biomarker Detection Directly in Blood Plasma

Andrea Ranzoni,[†,‡] Gwenola Sabatte,[†] Leo J. van IJzendoorn,[‡] and Menno W. J. Prins[†,‡,*]

[†]Philips Research, Eindhoven, The Netherlands, and [‡]Eindhoven University of Technology, The Netherlands

ABSTRACT

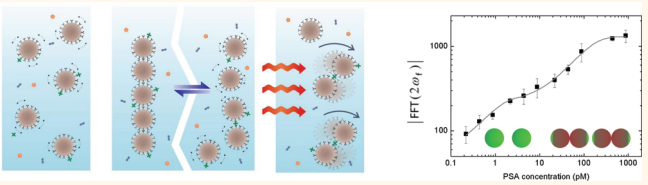

Assay technologies capable of detecting low biomarker concentrations in complex biological samples are fundamental for biological research and for applications in medical diagnostics. In this paper we address the challenge to perform protein biomarker detection homogeneously in one single step, applying a minute amount of reagent directly into whole human blood plasma, avoiding any sample dilution, separation, amplification, or fluid manipulation steps. We describe a one-step homogeneous assay technology based on antibody-coated magnetic nanoparticles that are spiked in very small amount directly into blood plasma. Pulsed magnetic fields and a double-linker molecular architecture are used to generate high biomarker-induced binding and low nonspecific binding between the nanoparticles. We demonstrate dose–response curves for prostate specific antigen (PSA) measured in undiluted human blood plasma with a detection limit of 400–500 femtomol/L, in a total assay time of 14 min and an optically probed volume of only 1 nL. We explain the dose–response curves with a model based on discrete binding of biomarker molecules onto the nanoparticles, which allows us to extract reaction parameters for the binding of biomarker molecules onto the nanoparticles and for the biomarker-induced binding between nanoparticles. The demonstrated analytical performance and understanding of the nanoparticle assay technology render it of interest for a wide range of applications in quantitative biology and medical diagnostics.

KEYWORDS: magnetic nanoparticles · one-step homogeneous immunoassay · whole human blood plasma · PSA

A biomarker is a molecular substance that can be measured and used as an indicator of a biological state. Technologies to detect biomarkers are essential for biological research and for applications in medical diagnostics. A common strategy in the design of biomarker assays is to use multiple sequential process steps, *e.g.* sample dilution, affinity capture, washing, labeling, and chemical or biochemical amplifications.[1−4] Disadvantages of a multistep strategy are that every additional step increases time, requires reagents, involves fluid manipulation, and introduces variability. Multistep assays can yield very high sensitivities, but they generally take hours to complete, use expensive reagents and sometimes lithographic chip technologies, and require complicated equipment. An opposite approach is to try to conceive and develop an assay technology that is based on only a single biofunctional probing reagent. Ideally, in a single step a very small amount of the probing reagent is spiked directly into the raw sample and a biomarker-dependent signal is acquired without needing any chip or any further reagents. Such a one-step homogeneous assay with minimal reagent use will be ideal for rapid measurements in small biological samples, provided that good biomarker detection sensitivities (*i.e.*, below the level of 1 picomol/L) can be realized in biological matrices such as blood plasma. Nanotechnological principles that may enable such a one-step homogeneous raw-sample assay with single reagent spike are, for example, biomarker-induced conformational changes in molecular probe molecules,[5−7] biomarker-induced binding between molecules[8] or between nanoparticles,[9−12] or conformational changes combined with interparticle binding.[13] However, raw biological samples are very difficult to deal with, particularly when dilution, washing, and amplification steps are avoided. Whole blood plasma for example contains very high levels and a wide variety of endogenous proteins,[14] which slow the transport of materials in the fluid and which drive nonspecific binding processes that can completely overwhelm the biological functionality of added assay reagents.

In this paper we describe a one-step homogeneous assay technology based on magnetic nanoparticles in a pulsed magnetic field. We demonstrate that the assay can be operated in undiluted human

* Address correspondence to menno.prins@philips.com.

Received for review December 15, 2011 and accepted March 13, 2012.

Published online March 13, 2012
10.1021/nn204913f

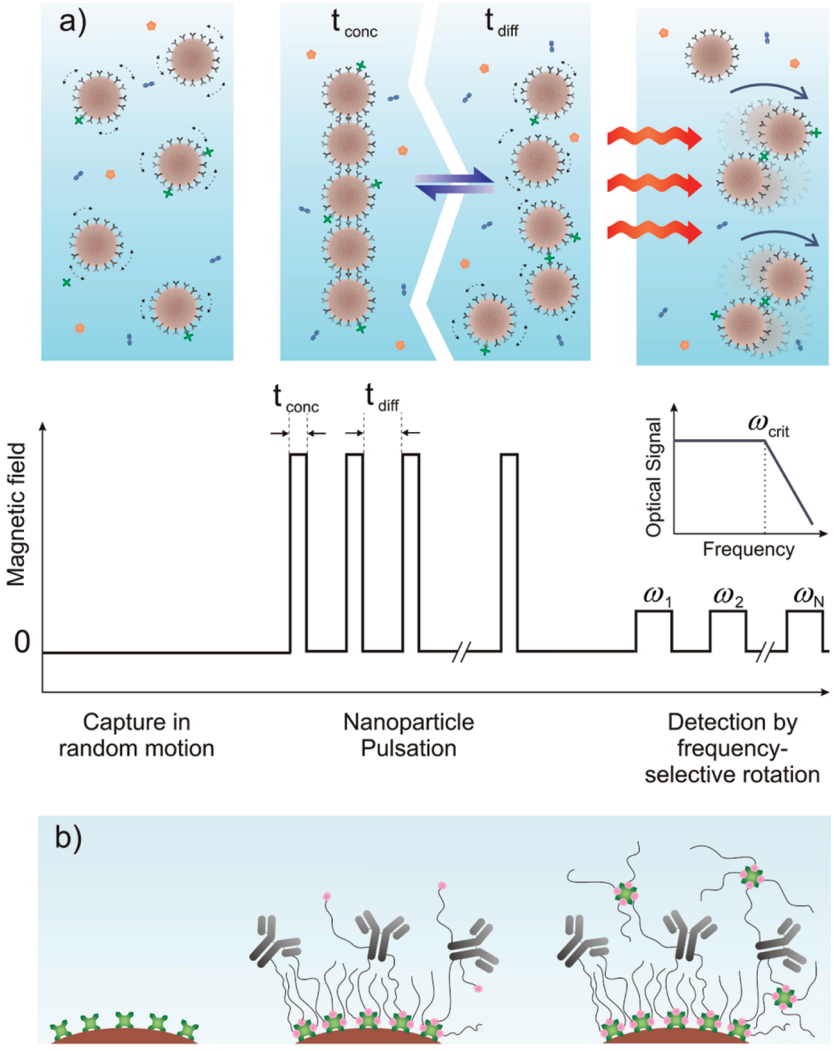

Figure 1. Principle of the one-step homogeneous assay technology based on magnetic nanoparticles. Into the biological sample a tiny volume of nanoparticle probing reagent is spiked, and thereafter the assay proceeds in three phases, which are controlled by the applied magnetic field (see panel a): Capture, pulsation, and detection. During the pulsation phase, nanoparticle concentration (t_{conc}) and nanoparticle diffusion (t_{diff}) are alternated, so that biomarker-induced nanoparticle clusters are formed. During the detection phase, the clusters are magnetically rotated and thereby generate a modulation of optical scattering. The result is a curve of optical scattering signal as a function of frequency (as sketched in the inset); the plateau reveals the number of clusters in solution, while the critical frequency reveals the cluster size and the viscosity of the sample.[16] (b) Scheme of the molecular surface architecture that we have engineered to suppress nonspecific interactions in complex matrices. Antibodies with biotinylated PEG (polyethylene glycol) linkers are coupled to streptavidin-coated nanoparticles. Thereafter a second layer of linkers is added in order to surround the antibodies by a shell of linkers.

plasma with high sensitivity and that the underlying assay processes can be quantitatively analyzed based on discrete molecular and nanoparticle binding events. The assay starts with the spiking of a very small amount of a nanoparticle probing reagent into the sample (typically a few volume percent). The nanoparticles are coated with monoclonal antibodies, targeting two different epitopes on the biomarker protein. After the one-step reagent spike, the assay proceeds in three phases as sketched in Figure 1a. In the first phase the biomarker molecules are captured by the antibody-coated magnetic nanoparticles in diffusive random motion, in the absence of a magnetic field. Thereafter a pulsating magnetic field alternatingly concentrates the particles in chains (during time t_{conc}) and lets the nanoparticles diffuse by Brownian motion (during t_{diff}). The field-on period generates a concentration of particles, while during the field-off period the diffusive motion randomizes the angular orientations of the nanoparticles and facilitates biomarker-induced inter-nanoparticle binding. The inter-nanoparticle binding gives clusters of nanoparticles, which are sensitively detected by optical scattering at applied magnetic rotation frequencies.[15,16] Curves are measured of the optical scattering signal as a function of the field rotation frequency (see the inset of Figure 1a), where the plateau signal reveals the number of clusters in solution and the value of the critical frequency, ω_{crit}, reveals the size of the clusters, as we will detail later. In our experiments the three phases of the assay take a

total time of 14 min, with 10 min for the capture phase, 2 min for pulsation, and 2 min for cluster detection.

We first investigate the binding dynamics of nanoparticles in a pulsating magnetic field. The assay is a sandwich immunoassay for prostate specific antigen (PSA), and we use a standard bioconjugation method (EDC coupling chemistry) to couple antibodies to carboxyl groups on the nanoparticles; details are given in the Methods section. The time and field required for the arrangement of nanoparticles into chains depend on the particle susceptibility and the particle density.[17] In our experiments we use a nanoparticle concentration of 1 pM, which corresponds to an average inter-nanoparticle distance of 12 μm. The particles with a diameter of 500 nm concentrate into chains very rapidly,[18] and in a magnetic field of 50 mT a concentration time t_{conc} of 2 s is sufficient. The role of nanoparticle diffusion in the inter-nanoparticle binding process can be studied by varying the diffusion time, t_{diff}, as presented in Figure 2a. The figure shows the optical scattering signal due to nanoparticle binding as a function of the diffusion time for a total of 20 applied pulses. The data show a steep signal rise at short diffusion times and a slight decrease at larger values. We can understand the steep rise from the time that is required for Brownian randomization of the nanoparticle orientations, which equals the time that is needed for translational diffusion by one particle diameter [55 ms for a 500 nm particle in water[19]]. The rotational and translational randomization increases the biomarker-induced binding probability of the nanoparticles by a factor of 2−3. This will result in an enhancement of biomarker detection sensitivity by more than an order of magnitude, due to the sublinear character of the dose−response curves, as we will see later in this paper. The decrease of inter-nanoparticle binding at long diffusion pulse widths ($t_{diff} > 4$ s) can be understood from the outward diffusion of the nanoparticles, which lowers the local nanoparticle concentration and thereby the encounter probability. We observe the same binding characteristics for different biomarker concentrations (see inset), which proves that the inter-nanoparticle binding dynamics are dominated by the properties of the nanoparticles and the applied field. Figure 2b shows the nanoparticle binding as a function of the total pulsation time. The nanoparticles are concentrated into chains during the first few pulses, and subsequently the binding signal rises and saturates. A Langmuir curve fit[20] reveals a time constant of $\tau = 37 \pm 10$ s. The time constant is independent of the biomarker concentration (see inset), which demonstrates that we operate in a regime where the antibodies on the nanoparticles rather than the biomarker molecules are limiting the inter-nanoparticle binding reaction. From the time constant we can estimate an effective biomarker-induced inter-nanoparticle association rate of $k_{on} \cong 10^4$ M^{-1} s^{-1} (see the Methods section).

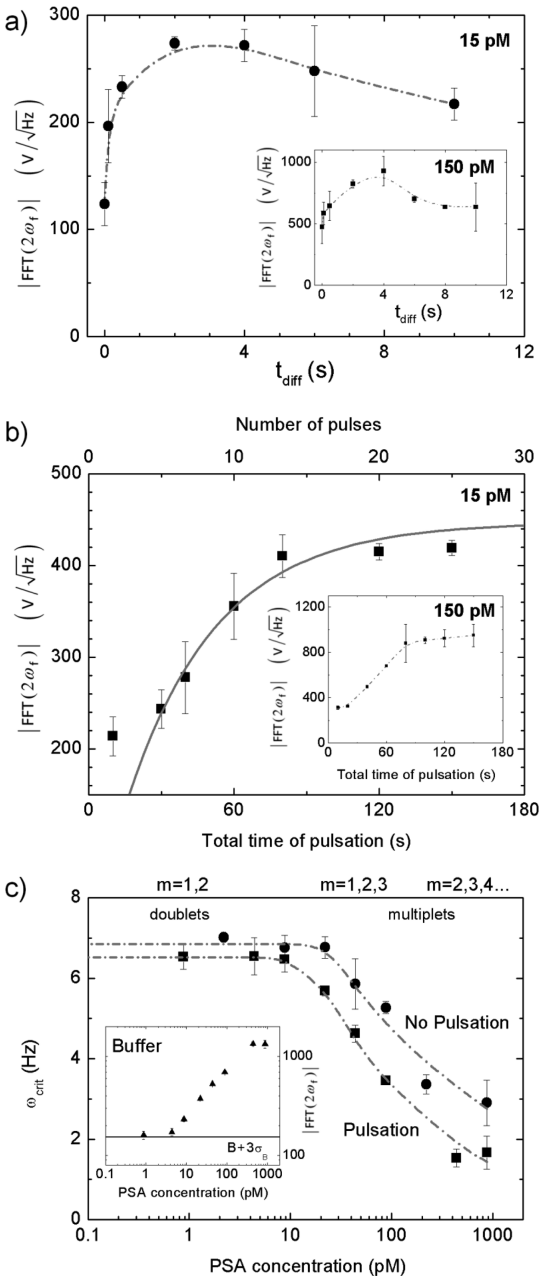

Figure 2. Nanoparticle binding as a function of magnetic pulse parameters. (a) Optical signal as a function of t_{diff}, the time for diffusive Brownian motion. The pulse width for nanoparticle concentration is t_{conc} = 2 s, and the total number of pulses is 20. The main panel shows data for a biomarker concentration of 15 pM; the inset, for 150 pM. (b) Nanoparticle binding signal as a function of the pulsation time. The solid line is a Langmuir curve with an association time constant of 37 s. (c) Critical frequency measured as a function of the biomarker concentration, for binding with pulsation (t_{diff} = 4 s) and without pulsation (t_{diff} = 0), in both cases for a field strength of 3.7 mT. The dashed lines are guides to the eye. The critical frequency is constant in the doublet regime (where m = 1 and m = 2) and drops as larger clusters appear (multiplet regime, m > 2).[16] The top x-axis indicates the cluster multiplicity number qualitatively observed by video microscopy. The inset shows a dose−response curve with pulsated nanoparticles, using a standard COOH surface chemistry. The horizontal line indicates the average value of the blank plus three times the standard deviation of the blank (N = 10). The dose−response curve shows a detection limit of 5 pM in buffer.

The inter-nanoparticle binding process generates an evolution of species in the fluid. The population starts with single nanoparticles. After biomarker capture and pulsation, two-particle clusters appear, denoted by the multiplicity number $m = 2$. The formation of two-particle clusters reduces the number of free single particles in solution. We speak of the doublet regime when the solution dominantly contains single particles and two-particle clusters ($m = 1$ and $m = 2$). We speak of the multiplet regime when clusters of higher multiplicity appear in solution ($m > 2$). At any time, the total signal S can be expressed as a summation over the species in solution: $S = \sum S_m N_m$, with S_m the signal per cluster and N_m the number of clusters with multiplicity m.

We can distinguish the doublet and multiplet regimes by recording the critical frequency of rotation. The critical rotation frequency, ω_{crit}, is the maximum applied rotation frequency that a cluster can synchronously follow (see the signal-*versus*-frequency inset in Figure 1a). The critical frequency depends on the cluster size; ω_{crit} is largest for $m = 2$, and it decreases for $m > 2$ because larger clusters have a larger viscous drag.[16] Figure 2c shows the critical frequency as a function of the biomarker concentration for an assay with and without pulsation. The development of the critical frequency is in agreement with observations of the cluster multiplicity by video microscopy (see top *x*-axis). The pulsation results in a dose–response curve with a detection limit of 5 pM in buffer (see inset). It appears that the system is in the multiplet regime over nearly the complete dose–response curve; so the standard bioconjugation method to couple antibodies to the nanoparticles appears to generate in buffer a high level of nonspecific binding, which masks the doublet regime in the dose–response data. The nonspecific nanoparticle binding increases further when blood plasma is used as a sample matrix, and as a result, picomolar biomarker concentrations cannot be resolved in this cluster assay.

In order to be able to investigate samples with subpicomolar biomarker concentrations in matrices of high biological complexity, we have developed a versatile molecular architecture as sketched in Figure 1b. Antibodies with flexible biotinylated linkers are attached to streptavidin-coated particles, and biotinylated linkers (without antibodies) are added to shield the surface of the nanoparticles and enhance the colloidal stability.[21] Thereafter another layer of linkers is added as an inert shell around the antibodies, coupled *via* multivalent streptavidin–biotin binding. We have studied linkers of different lengths and compared the modular architecture to the standard coupling of antibodies to carboxyl groups on the nanoparticles, showing a systematic increase of the hydrodynamic radius, a shift of the charge state, and a reduction of the nonspecific binding (see the Methods section). The surface architecture with a double layer of linkers very effectively suppresses the formation of nonspecific particle–particle bonds, significantly better than just a single layer of linkers. The pulsed magnetic assay reveals a pronounced effect of the surface architecture on the biomarker-induced binding of nanoparticles, as is shown in Figure 3. Panel (a) shows the critical frequency measured as a function of the biomarker concentration, in buffer and in untreated plasma. We see that a reliable low-concentration assay can now be performed in untreated plasma. The critical frequency in untreated plasma is about one-third of the value in buffer because of the higher viscosity of plasma (the critical frequency is inversely related to the fluid viscosity[15,16]). Figure 3b shows a dose–response curve recorded in buffer with the linker architecture on the nanoparticles. The nonspecific inter-particle binding is very effectively suppressed and results in a limit of detection of 160 femtomol/L PSA in buffer, which is about a factor of 30 lower than with the standard carboxyl coupling of antibodies to the nanoparticles. The inset shows that the nanoparticles have a time constant for inter-nanoparticle binding of only 12.7 ± 1.7 s, which is three times faster than with the standard bioconjugation method.

Interestingly, the dose–response curve reveals a shape with two undulations, one in the doublet regime and one in the multiplet regime (see Figure 3a). We can understand the shape from a model for the nanoparticle binding processes in the fluid (see Supporting Information). The model is based on the fact that the capturing of biomarkers by the nanoparticles is a discrete process governed by Poisson statistics. For low biomarker concentrations most nanoparticles do not carry a biomarker molecule, which gives a state with mainly single nanoparticles and only a few doublets. At high biomarker concentrations the binding probabilities increase, resulting in a state with many doublets and few single nanoparticles. For the doublet regime (with only $m = 1$ and $m = 2$) the total signal can be expressed as a function of the average number of biomarkers per nanoparticle x:

$$S(x) = \sum_m S_m N_m \cong S_2 \left[N_2^{ns} + (N - 2N_2^{ns}) \frac{1 - e^{-\xi x \Gamma}}{2 - e^{-\xi x \Gamma}} \right], \quad \text{with } \begin{matrix} x = C_b/C_N \\ \Gamma = 1 - e^{-t_{cap}/\tau_{cap}} \end{matrix} \tag{1}$$

where S_2 is the optical signal per doublet, N_2^{ns} is the number of doublets not caused by biomarkers (nonspecific doublet background), N is the total number of nanoparticles, ξ is the fraction of biomarkers on the nanoparticles that is sterically available to form an inter-nanoparticle bond ($0 \le \xi \le 1$), Γ is the fraction of biomarkers that is captured from solution onto the nanoparticles (Langmuir kinetics, $0 \le \Gamma \le 1$), C_b and C_N are respectively the concentration of biomarkers and

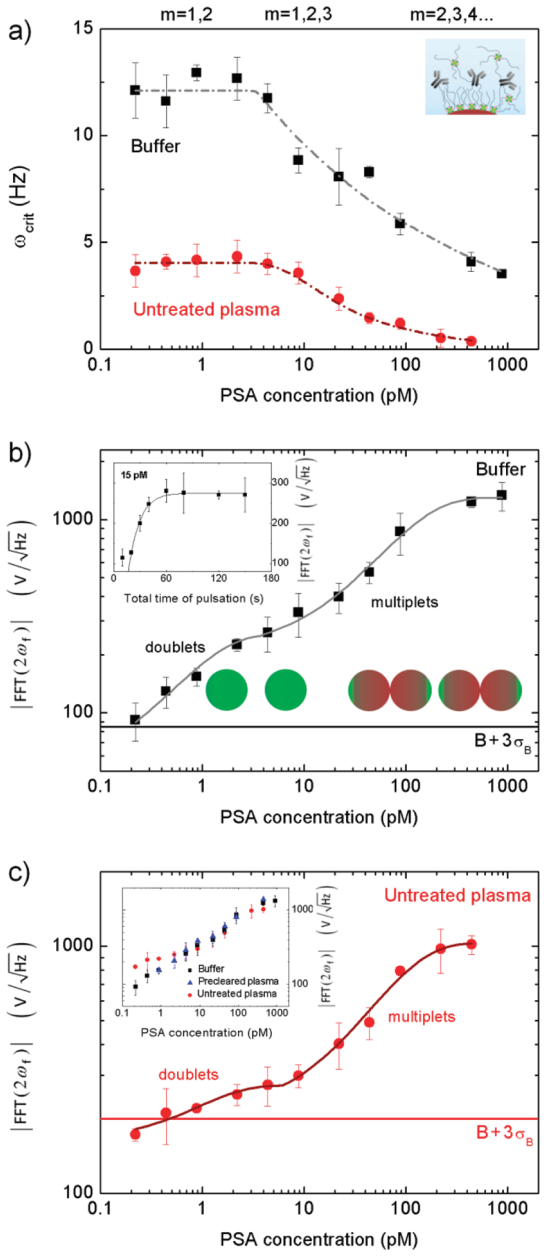

Figure 3. One-step homogeneous magnetic nanoparticle immunoassay for PSA, in buffer and in blood plasma. Nanoparticles are coated with the molecular surface architecture with linkers. The total reagent spike is only 5% of the plasma volume. (a) Critical rotation frequency of nanoparticle clusters as a function of the PSA concentration for buffer and untreated blood plasma, measured with a field of 6 mT. The dashed lines are guides to the eye. (b) Dose–response curve in buffer, where each point has been measured in triplicate. The doublet regime (up to 5 pM) has been fitted using eq 1; the curve fit in the multiplet regime is described in the Supporting Information. The inset shows the binding signal as a function of the pulsation time. The graphical sketch shows in green the effective areas for cluster growth, for single particles, and for doublets. (c) Dose–response curve in untreated blood plasma. The inset shows an overlay of the dose–response curves in buffer, precleared plasma, and untreated plasma. The line is a curve fit according to the model description (see the Supporting Information). The horizontal line shows the level of the blank plus three times the standard deviation of the blank.

nanoparticles in the original solution, t_{cap} is the duration of the biomarker capturing process, and τ_{cap} is the capture time constant. The steric availability factor ξ takes account of the fact that captured biomarker molecules have a limited potential to generate an inter-nanoparticle bond, due to steric hindrance originating from antibody misorientation or surface roughness of the particles. Figure 3b shows a fit of eq 1 to the data in the doublet regime. We have determined in an independent experiment that the captured fraction in buffer is about $\Gamma = 0.95$. This allows us to deduce from the curve fit that the biomarker steric availability for the surface architecture with linkers is $\xi = 0.43 \pm 0.12$, so about half of the captured biomarker molecules are sterically available to form an inter-nanoparticle bond. For the standard carboxyl coupling of antibodies, the steric availability is $\xi = 0.26 \pm 0.07$ (see Supporting Information), which is nearly a factor of 2 lower than for the surface architecture with linkers.

Interestingly the slope of the dose–response curve is the same for the doublet and the multiplet curve segments, but the multiplet segment is shifted toward higher biomarker concentrations. This points to a reduced binding effectiveness of multiplets *versus* single particles. We attribute the shift to a reduced effective area for elongation of multiplets. In the doublet regime, the formation of clusters is driven by single particles, whose spherical shape implies that biomarker molecules over their complete surface area can induce inter-nanoparticle binding. In the multiplet regime, the process to grow doublets into longer multiplets is sterically hindered, because the doublets are magnetically oriented and only biomarkers captured at their extremities can generate further cluster elongation (see sketch in Figure 3b). Consequently, the shape of a doublet causes a less effective biomarker-induced inter-nanoparticle binding process, which shifts the multiplet segment to higher concentrations in the dose–response curve. We can model the reduced binding effectiveness by an area ratio ρ, which is the ratio between the area of the two extremities and the total surface area of the cluster (see Supporting Information). From the fit we deduce an area ratio of $\rho = 0.012 \pm 0.005$, which points to the existence of effective binding caps with a solid angle of 0.65 sr. Note that an interesting consequence of the existence of the doublet and multiplet regimes is that the total assay dose–response curve has a very large dynamic range, over several orders of magnitude in biomarker concentration.

In Figure 3c we show dose–response data for assays in blood plasma, namely, for a mixed-gender plasma pool and for an untreated female plasma pool. The mixed-gender plasma pool was precleared by immuno-extraction of PSA originating from male plasma donors. Female plasma contains no or extremely low levels of PSA,[3] so PSA clearance was not required. The nanoparticle assay was performed with a reagent-to-plasma ratio of only 5%. The dose–response curve for the precleared plasma pool correlates perfectly with

the dose–response curve in buffer across three decades of biomarker concentration (see inset). Measurements in untreated female plasma also correlate well but show a higher blank level due to nonspecific binding. The limit of detection is 400–500 femtomol/L in both plasma types. A fit of the plasma dose–response data gives in plasma the same signal per doublet and the same effective binding cap as in buffer, but a slightly lower Langmuir factor ($\Gamma = 0.72 \pm 0.25$), which we attribute to the higher viscosity of the matrix.

CONCLUSION

We have described a one-step homogeneous immunoassay technology in which a very small amount of magnetic nanoparticles is spiked directly into whole blood plasma. Sensitive and rapid biomarker detection in blood plasma is enabled by the use of a pulsating magnetic field (see Figure 1a) and the use of a double-linker surface architecture on the nanoparticles (see Figure 1b). Both contribute in an essential manner to achieving high specific binding as well as low nonspecific binding in blood plasma. The dose–response curves consist of two concatenated segments, one in which nanoparticle doublets are formed and one in which multiplets are formed, which results in a dose–response curve with a dynamic range over several orders of magnitude in biomarker concentration. It is important to place our results in the perspective of existing literature. The founding paper of Baudry *et al.*[9] describes the enhancement of nanoparticle clustering by a magnetic field, but the paper shows assay results only for buffer and not for plasma. Our recent publication[16] describes the detection of magnetic nanoparticle clusters in a rotating magnetic field, but it shows only two-step assays (the samples were diluted in buffer halfway during the assay) and only for the binding of streptavidin to biotinylated BSA (bovine serum albumin). The latter is an artificial model system that has a binding affinity that is several orders of magnitude higher than the biological system of the present paper, *i.e.*, monoclonal antibodies capturing the medical biomarker PSA. Finally, papers that report high immunoassay sensitivities in plasma[1–4] use assays based on series of sequential processing steps (such as sample dilution, affinity capture, washing, labeling, and chemical or biochemical amplifications), use chip technologies,[4] and have very long total assay times. This is in strong contrast to the assay technology of this paper, which is based on only a single step, namely, the spiking of a small amount of probing reagent directly into a whole blood plasma sample, which uses an extremely small amount of reagent (few volume %), which does not need a chip technology (it is a homogeneous solution-based assay), and which has a total assay duration on the time scale of minutes. We have demonstrated the ability to record and model the population dynamics of the nanoparticle system and the ability to quantitatively extract the underlying parameters for capture of biomarkers onto the nanoparticles and for biomarker-induced inter-nanoparticle binding. We have demonstrated a limit of detection of 400–500 fmol/L PSA measured directly in whole human blood plasma, in a total assay time of 14 min and with an optical probing volume of only 1 nL. The optical probing volume is much smaller than the total sample volume of the cuvette used in the experiments. We have verified by video microscopy that the particles and particle clusters are uniformly distributed over the entire cuvette during the complete assay; therefore we foresee that the assay can also be performed in a much smaller sample volume, namely, a volume that is close to the present optical probing volume, *i.e.*, a sample volume on the order of a few nanoliters. The flexible magneto-temporal control of the homogeneous one-step assay, the fact that separation and washing steps are not necessary, the use of a single probing reagent in a very low amount, and the small sample volume render the technology suited for biological analysis and for further miniaturization, integration, and multiplexing. Ultrasmall samples can be taken and analyzed for biotechnological process monitoring[22] and the screening of libraries of biological materials.[23] The one-step homogeneous assay technology is also suited for medical *in vitro* diagnostics, in robotic high-throughput instrumentation, and in future rapid and cost-effective point-of-need systems that will operate with miniscule samples from a finger prick.[24–26] Furthermore, the experimental and modeling frameworks that we have developed in order to gain understanding of the underlying assay processes form a strong basis for further scientific studies on nanoparticle properties, coating properties, nanoparticle–matrix interactions, binding affinities, and the biological availability of surface-coupled antibodies, in buffer solutions as well as in complex biological matrices such as whole blood plasma.

METHODS

Opto-magnetic Platform. A collimated laser beam (658 nm wavelength, Sanyo DL-6147-240, operating at 15 mW) is focused with a low numerical aperture lens (NA = 0.025) into the center of a glass cuvette of square inner cross section (1 mm^2). The low numerical aperture lens gives a depth of focus of 1 mm, equal to the optical path inside the cuvette. The beam waist diameter is calculated to be $w = 1.22\lambda/NA = 32\,\mu m$. The optically probed fluid volume is approximately 1 nL. The focus of the laser beam and the center of the glass cuvette are placed in the middle of a quadrupole electromagnet, which generates a

rotating magnetic field in a vertical plane.[16] The electromagnets have been calibrated with a Hall probe and generate a maximum field of 70 mT. The self-inductance of the coils becomes important only at frequencies above several hundreds of Hz. We measure the scattered light at an angle of about 30° from the main optical axis, where the signal intensity is maximum. The scattered light is collected by a low NA lens onto a photodetector (New Focus, model 2031, gain 2.106). Voltage signals measured by the photodetector are sampled at 1 kHz during 3 s and stored in a file using digital data acquisition (National Instrument NI-DAQ 6259). The data are processed by an FFT algorithm in MATLAB to compute the signal amplitudes. The optical scattering signal from the clusters appears at twice the rotation frequency of the applied magnetic field, due to the point symmetry of the clusters. The fwhm value of the 2f peak is about 50 mHz. The precision of the 2f amplitude determination is better than 2%. Curves of the optical scattering signal as a function of frequency are determined between 1 and 25 Hz in a total scan time of 2 min. The signals are stable over time, indicating that no magnetically induced clusters are generated during the frequency-selective detection phase and that only the chemically formed clusters are measured.

Coating of COOH Nanoparticles with α-PSA Antibodies. Chemicals were purchased from Sigma Aldrich except if stated otherwise. EDC (1-ethyl-3-[3-dimethylaminopropyl]carbodiimide hydrochloride, Thermo Scientific Pierce) is dissolved in deionized water at a final concentration of 40 mg/mL. COOH magnetic nanoparticles (100 μL, AdemTech Masterbeads, 500 nm diameter) at 50 mg/mL are washed three times with 500 μL of MES buffer (50 mM MES buffer pH 6.2 + 0.001 [% v/v] Triton). The nanoparticles are suspended in 250 μL of MES buffer. The antibodies (α-PSA10 mAb and α-PSA66 mAb, purchased from Fujirebio) are added to the solution at a concentration of 20 μg per mg of nanoparticles, and EDC at a final concentration of 2 mg/mL is added. The nanoparticles are incubated for 30 min with the antibodies at room temperature, mixed on a thermomixer at 600 rpm. The reaction is blocked by adding 2 M Tris buffer pH 8.0 to a final concentration of 0.1 M. After 30 min the nanoparticles are magnetically washed twice and the supernatant is removed and replaced by 500 μL of 50 mM Tris buffer pH 8.0. As a last step, the nanoparticles are suspended in 500 μL of storage buffer (AdemTech). The binding kinetics of PSA to the antibodies has been measured by surface plasmon resonance (BiaCore SPR instrument), and a value of $k_{on} = 10^5\ M^{-1}\ s^{-1}$ was determined. We can estimate an effective k_{on} for biomarker-induced inter-nanoparticle binding from the data in Figure 2b. The data give a time constant of $\tau = 37 \pm 10$ s. From this time constant we can calculate an effective association rate $k_{on} = 1/(\tau C)$, with C the effective concentration of antibodies during the pulsation phase. We have determined the number of active antibodies per nanoparticle by incubating known amounts of nanoparticles and PSA for 1 h (long enough to reach equilibrium) and by measuring with UV absorption (Nanodrop) the amount of biomarker left in the supernatant. We found that each nanoparticle holds approximately 200 active antibodies. Thus the effective concentration of antibodies during the field-induced inter-nanoparticle binding process is approximately 200 per nanoparticle volume of about 500 nm cubed, so about 3 μM. This gives an estimate for the effective inter-nanoparticle association rate constant of $k_{on} \approx 10^4\ M^{-1}\ s^{-1}$.

Coupling of PEG Linkers to α-PSA Antibodies. Biotinylated PEG linkers modified with an NHS group (b-PEG-NHS, purchased from Creative PEG Works) were conjugated to the antibodies (α-PSA10 mAb and α-PSA66 mAb, purchased from Fujirebio). The concentration of antibodies was measured by UV absorbance (Thermo Scientific, Nanodrop). The b-PEG-NHS solution is prepared in PBS at 5 mM and is added to the antibodies in a 10 molar excess. The mixture is incubated for 1 h at room temperature under gentle shaking. The biotinylated antibodies are purified through a PD10 column in 0.1% NaN_3 in PBS. A control experiment with fluorescein-PEG-NHS linkers revealed that on average just a few PEG linkers are coupled to each antibody.

Linker Multilayer Architecture on Magnetic Nanoparticles. Streptavidin-coated nanoparticles (10 mg/mL; 500 nm Masterbeads, AdemTech, 6×10^{10} particles per mL) are magnetically washed three times in PBS buffer and resuspended in PBS by sonicating three times at 50 W for 3 s. A 25 μg amount of biotinylated α-PSA antibodies per milligram of nanoparticles is added to the nanoparticles and incubated for 15 min under gentle shaking. Additional hydrolyzed b-PEG-NHS (thus with a nonreactive NHS group) is added to the solution at a final concentration of 200 pmol per milligram of nanoparticles and incubated for 15 min under gentle shaking. An excess of streptavidin (2.2 nmol per mg nanoparticles) is added and incubated under gentle shaking for 10 min, and then an excess of hydrolyzed b-PEG-NHS (90 nmol per mg nanoparticles) is added and incubated for 15 min under gentle shaking. The nanoparticles are magnetically washed and suspended in buffer (5% BSA in PBS with 1 mM biotin). The solution is sonicated for 3 s at 50 W.

Measurement of Mean Nanoparticle Size and Charge. Measurements have been performed by dynamic light scattering (Malvern, Zetasizer). For measuring the hydrodynamic mean diameter, the nanoparticles have been diluted to 50 μg/mL in NaCl buffer, and a sample volume of 1 mL was sonicated at 50 W for 3 s twice. The mean diameter progressively increases, from 506 nm (COOH) to 520 nm (Streptavidin) and to 550 nm (PEG-coated nanoparticles). The same protocol has been followed for the zeta potential measurements, using 10 mM phosphate buffer pH 7.4. The measurements show a progressive reduction in the surface charge of the nanoparticles: carboxyl-coated nanoparticles are most strongly charged ($Z = -23$ mV), then the particles with streptavidin ($Z = -19$ mV), and the particles with PEG linkers have the lowest charge ($Z = -14$ mV). In buffer, only the PEG-coated nanoparticles showed no measurable nonspecific interparticle binding, which demonstrates that PEG linkers suppress nonspecific interactions and increase the nanoparticle stability.

Immunoassay Samples. We performed immunoassay experiments in three matrices, namely, in buffer, in a mixed-gender plasma pool that was precleared of PSA, and in an untreated female plasma pool:

(1) Experiments in buffer. PSA is spiked in buffer (5% BSA in PBS) from a PSA calibrator (60 μg/L) purchased from Fujirebio. In the immunoassay experiments, 1.5 μL of α-PSA nanoparticles at 2 mg/mL (1:1 ratio of α-PSA10 mAb and α-PSA66 mAb nanoparticles) is added to 28.5 μL of buffered PSA.

(2) Experiments in mixed-gender heparin plasma pool (purchased from Innovative). Mixed-gender plasma pools contain a background PSA level from male plasma donors. We cleared the plasma by incubating for 30 min a volume of 0.5 mL of plasma with 5 mg of nanoparticles coated with α-PSA antibodies and subsequently with 5 mg of nanoparticles coated with Protein G to remove excess IgG. The nanoparticles are magnetically removed, and the precleared plasma is spiked with PSA from the calibrator. The immunoassay capture starts by adding α-PSA nanoparticles to the sample, with 1.5 μL of nanoparticles at 2 mg/mL added to 28.5 μL of precleared plasma. The solution has a final plasma content of 95%.

(3) Experiments in female heparin plasma pool (from SeraLab). Female plasma contains no or extremely low levels of PSA, so PSA clearance is not required. The plasma is spiked with PSA from the calibrator and a detergent at 2% w/v in dry form. The immunoassay capture starts by adding α-PSA nanoparticles to the sample, with 1.5 μL of nanoparticles at 2 mg/mL added to 28.5 μL of plasma. The solution has a final plasma content of 95%.

Conflict of Interest: The authors declare no competing financial interest.

Acknowledgment. This work was partially funded by The Netherlands Ministry of Economic Affairs *via* the MicroNed program. We thank J. Schleipen and A. van Reenen for their advice and critical reading of the manuscript.

Supporting Information Available: A derivation of the equations for nanoparticle cluster formation is described. This material is available free of charge *via* the Internet at http://pubs.acs.org.

REFERENCES AND NOTES

1. Fredriksson, S.; Gullberg, M.; Jarvius, J.; Olsson, C.; Pietras, K.; Gustafsdottir, S. M.; Ostman, A.; Landegren, U. Protein Detection Using Proximity-Dependent DNA Ligation Assays. *Nat. Biotechnol.* **2002**, *20*, 473–477.
2. Todd, J.; Freese, B.; Lu, A.; Held, D.; Morey, J.; Livingston, R.; Goix, P. Ultrasensitive Flow-Based Immunoassays Using Single-Molecule Counting. *Clin. Chem.* **2007**, *53*, 1990–1995.
3. Thaxton, C. S.; Elghanian, R.; Thomas, A. D.; Stoeva, S. I.; Lee, J.-S.; Smith, N. D.; Schaeffer, A. J.; Klocker, H.; Horninger, W.; Bartsch, G.; Mirkin, C. A. Nanoparticle-Based Bio-Barcode Assay Redefines "Undetectable" PSA and Biochemical Recurrence after Radical Prostatectomy. *Proc. Natl. Acad. Sci. U. S. A.* **2009**, *106*, 18437–18442.
4. Rissin, D. M.; Kan, C. W.; Campbell, T. G.; Howes, S. C.; Fournier, D. R.; Song, L.; Piech, T.; Patel, P. P.; Chang, L.; Rivnak, A. J.; *et al.* Single-Molecule Enzyme-Linked Immunosorbent Assay Detects Serum Proteins at Subfemtomolar Concentrations. *Nat. Biotechnol.* **2010**, *28*, 595–599.
5. Golynskiy, M. V.; Koay, M. S.; Vinkenborg, J. L.; Merkx, M. Engineering Protein Switches: Sensors, Regulators, and Spare Parts for Biology and Biotechnology. *Chem. Biochem.* **2011**, *12*, 353–361.
6. Vinkenborg, J. L.; Karnowski, N.; Famulok, M. Aptamers for Allosteric Regulation. *Nat. Chem. Biol.* **2011**, *7*, 519–527.
7. Vallee-Belisle, A.; Plaxco, K. W. Structure-Switching Biosensors: Inspired by Nature. *Curr. Opin. Struct. Biol.* **2010**, *20*, 518–526.
8. Zhou, X.; Tang, Y.; Xing, D. One-Step Homogeneous Protein Detection Based on Aptamer Probe and Fluorescence Cross-Correlation Spectroscopy. *Anal. Chem.* **2011**, *83*, 2906–2912.
9. Baudry, J.; Rouzeau, C.; Goubault, C.; Robic, C.; Cohen-Tannoudji, L.; Koenig, A.; Bertrand, E.; Bibette, J. Acceleration of the Recognition Rate Between Grafted Ligands and Receptors with Magnetic Forces. *Proc. Natl. Acad. Sci. U. S. A.* **2006**, *103*, 16076–16078.
10. Lee, H.; Sun, E.; Ham, D.; Weissleder, R. Chip-NMR Biosensor for Detection and Molecular Analysis of Cells. *Nat. Med.* **2008**, *14*, 869–874.
11. Mitchell, S. W.; Mboup, S.; Mingle, J.; Sambe, D.; Tukei, P.; Milenge, K.; Nyamongo, J.; Mubarak, O. K.; Sankale, J. L.; Hanson, D. S.; Quinn, T. C. Field-Evaluation of Alternative HIV Testing Strategy with a Rapid Immunobinding Assay and an Agglutination Assay. *Lancet* **1991**, *337*, 1328–1331.
12. Sulahian, A.; Tabouret, M.; Ribaud, P.; Sarfati, J.; Gluckman, E.; Latge, J. P.; Derouin, F. Comparison of an Enzyme Immunoassay and Latex Agglutination Test for Detection of Galactomannan in the Diagnosis of Invasive Aspergillosis. *Eur. J. Clin. Microbiol. Infect. Dis.* **1996**, *15*, 139–145.
13. Maye, M. M.; Kumara, M. T.; Nykypanchuk, D.; Sherman, W. B.; Gang, O. Switching Binary States of Nanoparticle Superlattices and Dimer Clusters by DNA Strands. *Nat. Nanotechnol.* **2010**, *5*, 116–120.
14. Anderson, N. L.; Anderson, N. G. The Human Plasma Proteome—History, Character, and Diagnostic Prospects. *Mol. Cell. Proteomics* **2002**, *1*, 845–867.
15. Ranzoni, A.; Janssen, X. J. A.; Ovsyanko, M.; van IJzendoorn, L. J.; Prins, M. W. J. Magnetically Controlled Rotation and Torque of Uniaxial Microactuators for Lab-on-a-Chip Applications. *Lab Chip* **2010**, *10*, 179–188.
16. Ranzoni, A.; Schleipen, J. J. H. B.; van IJzendoorn, L. J.; Prins, M. W. J. Frequency-Selective Rotation of Two-Particle Nanoactuators for Rapid and Sensitive Detection of Biomolecules. *Nano Lett.* **2011**, *11*, 2017–2022.
17. Calderon, F. L.; Stora, T.; Monval, O. M.; Poulin, P.; Bibette, J. Direct Measurement of Colloidal Forces. *Phys. Rev. Lett.* **1994**, *72*, 2959–2962.
18. Promislow, J. H. E.; Gast, A. P.; Fermigier, M. Aggregation Kinetics of Paramagnetic Colloidal Particles. *J. Chem. Phys.* **1995**, *102*, 5492–5498.
19. Astalan, A. P.; Ahrentorp, F.; Johansson, C.; Larsson, K.; Krozer, A. Biomolecular Reactions Studied Using Changes in Brownian Rotation Dynamics of Magnetic Particles. *Biosens. Bioelectron.* **2004**, *19*, 945–951.
20. Squires, T. M.; Messinger, R. J.; Manalis, S. R. Making It Stick: Convection, Reaction and Diffusion in Surface-Based Biosensors. *Nat. Biotechnol.* **2008**, *26*, 417–426.
21. Cruz, L. J.; Tacken, P. J.; Fokkink, R.; Figdor, C. G. The Influence of PEG Chain Length and Targeting Moiety on Antibody-Mediated Delivery of Nanoparticle Vaccines to Human Dendritic Cells. *Biomaterials* **2011**, *32*, 6791–6803.
22. Mattiasson, B.; Teeparuksapun, K.; Hedstrom, M. Immunochemical Binding Assays for Detection and Quantification of Trace Impurities in Biotechnological Production. *Trends Biotechnol.* **2009**, *28*, 20–27.
23. Theberge, A. B.; Courtois, F.; Schaerli, Y.; Fischlechner, M.; Abell, C.; Hollfelder, F.; Huck, W. T. S. Microdroplets in Microfluidics: An Evolving Platform for Discoveries in Chemistry and Biology. *Angew. Chem., Int. Ed.* **2010**, *49*, 5846–5868.
24. Wild, D. *The Immunoassay Handbook*, 2nd ed.; Nature Publishing Group: 2001.
25. Martinez, A. W.; Phillips, S. T.; Whitesides, G. M.; Carrilho, E. Diagnostics for the Developing World: Microfluidic Paper-Based Analytical Devices. *Anal. Chem.* **2010**, *82*, 3–10.
26. Yager, P.; Edwards, T.; Fu, E.; Helton, K.; Nelson, K.; Tam, M. R.; Weigl, B. H. Microfluidic Diagnostic Technologies for Global Public Health. *Nature* **2006**, *442*, 412–418.